Ocean Dynamics (2014) 64:143–157
DOI 10.1007/s10236-013-0664-7

# Flocculation and particle size analysis of expansive clay sediments affected by biological, chemical, and hydrodynamic factors

**Xiaoling Tan · Liming Hu · Allen H. Reed · Yoko Furukawa · Guoping Zhang**

Received: 4 March 2012 / Accepted: 20 October 2013 / Published online: 21 November 2013
© Springer-Verlag Berlin Heidelberg 2013

**Abstract** Expansive clay sediments are abundant in riverine and estuarine waters and bottom beds, and their particle size distributions (PSD) are important for the analysis of sediment transport. This paper presents an experimental study to evaluate, using a laser particle size analyzer under varying flow conditions, the intrinsic PSD of two expansive clays, a Ca- and a Na-montmorillonite and the influence of biological, chemical, and hydrodynamic factors on their flocculation and PSD. The considered biological factor consists of three extracellular polymeric substances of varying polarity, including xanthan gum, guar gum, and chitosan; the chemical factor is the salinity; and the hydrodynamic factor is the types of flow indicated by the Reynolds number and shear rate. The intrinsic PSD of both clays show a multimodal lognormal distribution with sizes ranging from 0.2 to 50 μm. All three biopolymers, xanthan gum, guar gum, and chitosan, can facilitate flocculation through long-range polymer bridging and short-range ion-dipole interaction, hydrogen bonding, and Coulomb force. The influence of salinity is different for the two clays: the particle size of the Na-montmorillonite increases with salinity, which is caused by flocculation resulting from the suppressed electrical double layer, while that of the Ca-montmorillonite is slightly reduced owing to the decreased basal spacing and cation exchange. For different hydrodynamic conditions, higher shear rate promotes the flocculation of Ca-montmorillonite, but breaks the Na-montmorillonite flocs. The significance of understanding the flocculation and PSD of expansive clays is also discussed in terms of sediment transport under different aquatic environments.

**Keywords** Extracellular polymeric substances · Expansive clays · Flocculation · Hydrodynamics · Particle size · Salinity

Responsible Editor: Qing He

This article is part of the Topical Collection on the *11th International Conference on Cohesive Sediment Transport*

X. Tan · G. Zhang (✉)
Department of Civil and Environmental Engineering,
Louisiana State University, Baton Rouge, LA 70803, USA
e-mail: zhangg@umass.edu

G. Zhang
e-mail: gzhang@alum.mit.edu

L. Hu
State Key Laboratory of Hydro-Science & Engineering, Department of Hydraulic Engineering, Tsinghua University,
Beijing 100084, China

A. H. Reed · Y. Furukawa
Naval Research Laboratory,
Stennis Space Center, MS 39529, USA

## 1 Introduction

Expansive clay sediments, such as smectite, vermiculite, and other mixed layer clays, are abundant in riverine and estuarine waters and bottom beds (Nair et al. 1982; Seo et al. 2009). For instance, the fine-grained marine sediment in deep Gulf of Mexico contains 26.2 wt% smectite of all clay minerals (other non-expansive ones include 44.7 wt% illite, 11.4 wt% kaolinite, and 17.7 wt% chlorite) (Devine et al. 1972), and in the cohesive sediments from Mississippi River estuary, there are as much as 45 wt% montmorillonite, but only 17 wt% illite and 12 wt% kaolinite (Hiltabrand et al. 1973). As a member of the smectite group, montmorillonite is the well-known and most common expansive clay. Basically, these clays, different from those non-swelling counterparts (e.g., kaolinite, illite, chlorite), expand or swell when they gain water and shrink when they lose water. According to the crystal structure, these clays belong to the 2:1 layer type with each layer consisting of two tetrahedral (T) silica sheets sandwiching a central octahedral (O) alumina sheet (Fig. 1). Due to isomorphous substitutions such as the $Si^{4+}$ by $Al^{3+}$ in the T sheet and/or $Al^{3+}$ by

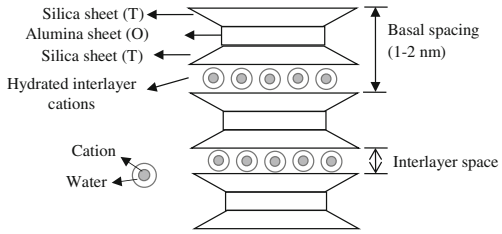


**Fig. 1** A schematic diagram showing the montmorillonite structure

$Mg^{2+}$ in the O sheet, these naturally occurring clays have permanent negative charges on face surfaces, which are balanced by positive counterions (also called "interlayer cations") adsorbed onto face surfaces. In these swelling clays, the interlayer cations are usually hydrated and also function as bonds to hold together adjacent 2:1 layers, resulting in relatively weak bonding. Smectite clays with $Na^{+}$ or $Ca^{2+}$ interlayer cations usually exhibit a higher expansive capability. Therefore, for these clays, the potential of water penetration into the interlayer spacing is much higher compared with those non-swelling kaolinite, illite, and chlorite (Luckham and Rossi 1999). Additionally, at the edge surface of each clay, the broken Si–O and Al–O covalent bonds expose and bestow them a pH-dependent charge: positive and negative in acidic and alkaline conditions, respectively (van Olphen 1964).

Cohesive sediments usually exhibit a wide range of particle sizes even in pure water at a steady state condition, owing to their special properties such as irregular particle shape, flexible layer, heterogeneous layer charge, pH-dependent edge charge, and various modes of flocculation (Murray 2000; Wu 2001; Lagaly and Ziesmer 2003). For expansive clays, their swelling nature also renders them to change their sizes with swelling, and different interlayer cations can further alter the degree of swelling (Kleijn and Oster 1982) and hence particle sizes. The natural sediment–water system is usually loaded with various types of organic matter, background ions, and flow conditions, which can further alter the aggregation or flocculation of expansive clays by different mechanisms (Hill 1998; Mietta et al. 2009). Complex change in the particle size of expansive clays can result from the increase in interlayer space, layer exfoliation, and flocculation under different biological, chemical, and hydrodynamic conditions. Besides, flocculation and associated size change usually generate flocs with relatively smaller density in the order of 50–300 $kg/m^3$ (Winterwerp 1998), which alters the settling velocity and hence the transport and fate of cohesive sediment. Knowledge of their intrinsic particle size distributions (PSD) and variations in different biological, chemical, and hydrodynamic conditions is of key importance to the understanding of sediment hydrodynamics and transport in natural waters, nutrient or contaminant removal from water column, and the influence of involved organic matter on sediment yield (Hill 1998; Chang et al. 2006; van Leussen 2011).

One type of the abundant, naturally occurring organic matter is the extracellular polymeric substances (EPS), which may vary significantly in different seasons and locations. Their concentration in natural waters typically ranges from 0 to ~1,000 μg/g (Hirst et al. 2003; Gerbersdorf et al. 2009). Owing to the chemically active surfaces of clays, EPS can interact extensively with clay particles via a series of mechanisms, including polymer bridging, polymer intercalation into the interlayer space of expandable clays, ion–dipole interaction on clay surfaces, hydrogen bonding, and electrostatic forces (Theng 1982; Lagaly et al. 2006). Depending upon their type, concentrations, and polarity, EPS can facilitate the flocculation of clay sediments and hence result in the change in the PSD. Moreover, the existence of permanent negative charges on clay face surfaces results in the formation of an electrical double layer (DL), which can be altered by the concentration of cations or salinity in the suspension liquid. The pronounced cation exchange capacity (CEC) of expansive clays also enables the exchange of the interlayer cations with different background cations, resulting in swelling or shrinkage. Therefore, the presence of salt (including different ions) in riverine or estuarine waters can lead to the compression of the DL as well as the exchange of interlayer cations, and hence the flocculation of primary clay particles or strengthening of the clay flocs may take place. The stability and strength of clays flocs can in turn change the PSD under different hydrodynamic conditions that can exert flow-induced shear stress to breakup larger flocs into smaller ones or help grow smaller flocs into larger ones (Yeung et al. 1997; Jarvis et al. 2005).

Due to the distinct crystal structure and properties of expansive clays, their particle sizes are more sensitive to different solvents and environmental conditions. Additionally, the natural water systems are usually very complex, and the in situ monitoring of cohesive sediment flocculation behavior is difficult. Therefore, this paper presents a laboratory study of the flocculation behavior and particle size change of expansive clay sediments under controlled conditions in order to isolate different factors influencing the flocculation of expansive clays. The major objective of this study was to characterize the intrinsic PSD and their variations of two common swelling clays, a Ca- and a Na-montmorillonite, affected by different dispersion methods, different solvents, as well as the presence of EPS, salt, and different hydrodynamic conditions.

## 2 Materials and methods

The flocculation behavior and PSD of two selected expansive clays were characterized by a laser based particle size analyzer installed with a liquid circulation system. To evaluate their intrinsic PSD, different dispersion methods, including dispersing in solvents of varied polarity (i.e., water and alcohol), with

and without chemical dispersant or ultrasound disintegration, and dry dispersing in air. Three different EPS at various concentrations were selected to evaluate the influence of biological factors on their PSD. Salt water with different, gradient salinities was then used to study the influence of chemical factors. Finally, the hydrodynamic conditions were varied by controlling the flow speed in the liquid circulation system of the particle size analyzer. In summary, a total of 10 particle size tests (two samples and five dispersion methods for each sample) was performed to measure the intrinsic PSD, and of 90 tests to characterize the influences of three different EPS at three concentrations, four salinities, and three hydrodynamic conditions on the PSD of two clays.

## 2.1 Materials

### *2.1.1 Expansive clays*

Two members of montmorillonite, a Ca-montmorillonite (Ca-M) and a Na-montmorillonite (Na-M), from the US Clay Minerals Society Source Clay Repository, were chosen as the representatives of the limited and unlimited swelling clays, respectively. Their geographic origin and basic properties are summarized in Table 1. The main interlayer cations are $Ca^{2+}$ for Ca-M and $Na^{+}$ for Na-M, which are both hydrated in these two clays. Na-M swells much more than Ca-M in suspensions, which could lead the formation of exfoliated 2:1 layers as individual particles. However, in a nonpolar or less polar liquid such as ethyl alcohol, these two clays do not readily swell.

### *2.1.2 Chemical reagents*

To evaluate the influence of different chemical factors on the PSD and hence obtain the intrinsic PSD of the two clays, deionized (DI) water, ethyl alcohol (EA), and Na-hexametaphosphate (NaHMP) were selected as a polar solvent, less polar solvent, and chemical dispersant, respectively, to prepare clay suspensions for subsequent particle size analysis. The alcohol, 190 Proof (95 % purity), was purchased from Pharmco-AAPER. The NaHMP was obtained from Mallinckrodt Baker Inc., Philipsburg, NJ. According to the American Society for Testing and Materials (ASTM) Method D422-63 (D422-63 2007), a NaHMP solution with a concentration of 40 g/L was used as the liquid for clay suspension preparation. In addition, an Instant Ocean® sea salt was chosen to prepare clay suspensions with varied salinities.

### *2.1.3 EPS*

Interaction of clay and EPS typically depends on the charge or polarity of EPS, thus EPS can be roughly classified into three types: anionic, neutral, and cationic (Theng 2012). To account for a variety of microbial EPS in natural waters, polyanionic xanthan gum (Spectrum®, Gardena, CA), neutral guar gum (Fisher ChemAlert® Guide, Rochester, NY), and polycationic chitosan (Acros Organics, New Jersey, USA) were chosen as the EPS representatives that may induce flocculation of clay sediments. In fact, all of the three EPS have been widely used and studied as coagulants (Yokoi et al. 1996; Yokoi et al. 1998; Majeti and Kumar 2000; Sashiwa and Aiba 2004; Gupta and Ako 2005; Chen and Chung 2011). Their chemical structure is shown in Fig. 2. Xanthan gum is a water-soluble bacterial extracellular polysaccharide produced through fermentation by *Xanthomonas campestris* bacterium. Due to different bacterial strains and the growth environments, the molecular weight of xanthan varies but typically ranges 0.9–$1.6\times10^6$ Da (Ian 1994). As shown in Fig. 2a, xanthan consists of $\beta$-(1,4)-*D*-glucopyranose glucan backbone with extended side chains of (3→1)-$\alpha$-linked *D*-mannopyranose-(2→1)-$\beta$-*D*-mannopyranose on alternating residues. Its negative charge is from the carboxylic acid groups (−COOH) in glucuronic acid and pyruvic acid groups on side chains (Ian 1994). Guar gum is a water-soluble polysaccharide extracted from guar beans with a molecular weight of up to $2\times10^6$ Da (Risica et al. 2005; Nugent et al. 2009). It is not a true exopolymer, but usually used as an EPS analog representative of neutral microbial exopolymers. Guar gum structurally consists of long,

**Table 1** Origin and basic properties of the two expansive clays

| Name | Origin | CEC (meq/100 g) | Layer charge[a] (unbalanced) | SSA ($m^2$/g) | pH[b] | Chemical formula |
|---|---|---|---|---|---|---|
| Ca-montmorillonite (STx-1b) | Gonzales County, Texas | 84.4 | −0.34 (−0.04) | 83.79 | 6.44 | $(Ca_{.27}Na_{0.04}K_{.01})[Al_{2.41}Fe^{3+}{}_{0.09}Mn_{tr}Mg_{0.71}Ti_{0.03}][Si_{8.00}]O_{20}(OH)_4$ |
| Na-montmorillonite (SWy-2) | Crook County, Wyoming | 76.4 | −0.28 (+0.025) | 31.82 | 7.32 | $(Ca_{0.12}\ Na_{0.32}K_{0.05})\ [Al_{3.01}\ Fe^{3+}{}_{0.41}\ Mn_{0.01}Mg_{0.54}Ti_{0.02}]\ [Si_{7.98}\ Al_{0.02}]\ O_{20}(OH)_4$ |

All data are from the Clay Minerals Society Source Clay Data Sheets

*SSA* specific surface area

[a] The layer charge is based on per $O_{10}(OH)_2$ unit

[b] pH of clay suspension at a concentration of 0.4 g/L in deionized water

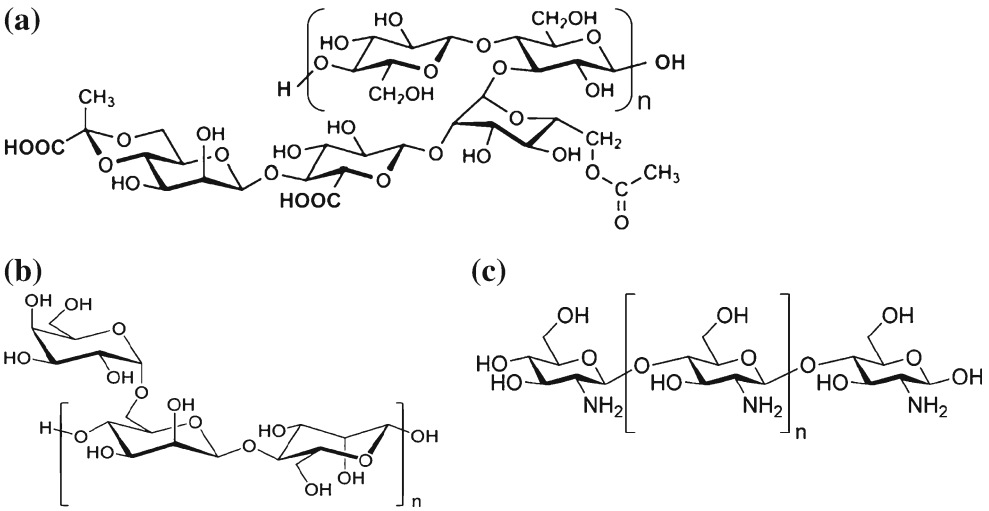


**Fig. 2** Chemical structure of **a** xanthan gum, **b** guar gum, and **c** (100 % deacetylated) chitosan

liner chains of $\alpha$-*D*-manopyranosyl units linked together by $\beta$-*D*-(1,4)-glycosidic linkage mannose residues with a $\alpha$-(1,6) linked *D*-galactose. There are 1.5–2 mannose residues for every galactose residue in average. Upon dissolving, guar gum can produce viscous, pseudoplastic aqueous solutions. Chitosan is obtained from the deacetylation process of chitin, which is the supporting material of shrimp and crab shells and other crustaceans or insects (Majeti and Kumar 2000). It is composed of $\beta$-(1,4) linked *D*-glucosamine without side chains. The molecular weight is $1–3\times10^5$ Da, and its positive charge is from the hydrolysis of amino groups in water.

## 2.2 Preparation and size analysis of clay suspensions

The PSD of the two expansive clay samples and clay–EPS mixtures was characterized by a Cilas® 1190 particle size analyzer (PSA) (Cilas Particle Size, Madison, WI, USA) (Fig. 3). This instrument can perform measurement in both liquid mode and dry mode. In the liquid mode, a sample is dispersed in a liquid (usually water) bath assisted by a stirrer and/or a built-in ultrasound disperser, and then the suspension is continuously circulated by a peristaltic pump whose speed can be varied. The dry mode is designed to measure the PSD of dry powdery samples without the need of preparing a suspension. Instead, a dry powdery sample is directly placed in the vibrating bowl of a mass distributor. The optimal dispersing parameters, including the vibrator's frequency and cyclic ratio of vibration, and air pressure are usually obtained by trial and error. In this work, the dry mode was only chosen to evaluate the intrinsic PSD of the two expansive clays.

Both pure clay and clay–EPS suspensions were prepared for size analysis under the liquid mode. For each of the two clays, 0.2 g dry powder was soaked overnight with DI water, followed by dilution with DI water into a 500 mL (which was the total volume of the PSA's liquid circulation system, including the liquid bath and connecting pipes) clay suspension with a final concentration of 0.4 g/L in the PSA liquid system while both the stirrer and pump were running at their lowest speed. The flow pattern inside this PSA liquid circulation system is very complex because it consists of several different

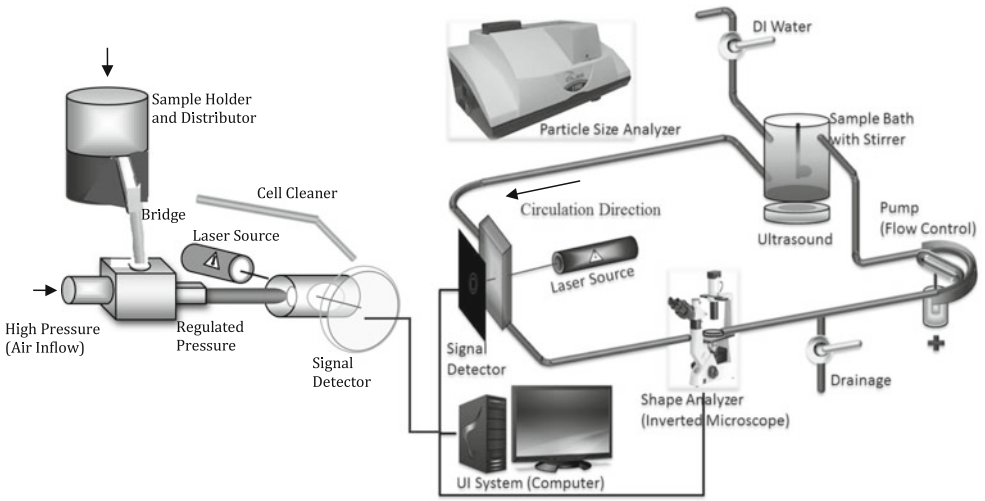


**Fig. 3** Schematic diagrams of dry mode system (*left*) and liquid dispersion and circulation system (*right*) in the PSA

sections with different flow areas (i.e., the stirring bath, flow pipe, connection parts, the laser diffraction and optical microscope observation windows, and squeezed section of the pipe in the peristaltic pump). Therefore, different flow conditions are expected to take place in different sections of the pipe. However, because other sections were very short and hence their effects could be ignored, only the hydrodynamic conditions of flow in the stirring bath and pipe were specifically considered in this study. Reynolds number ($R_e$) and average shear rate ($G$) of these two parts were calculated as follows:

1. In the stirring bath

   According to Camp and Stein (1943) and Spicer and Pratsinis (1996), the Reynolds number is

$$R_e = \frac{\rho \times \Omega \times D_A^2}{\mu} \tag{1}$$

   and the average shear rate is

$$G = \sqrt{\frac{\overline{\varepsilon}}{v}} \tag{2}$$

   and $\overline{\varepsilon}$ , the average turbulent energy dissipation per unit time and mass, is

$$\overline{\varepsilon} = \frac{N_p \times \Omega^3 \times D_A^5}{V} \tag{3}$$

   where $\rho$ is the fluid density, $\Omega$ the angular velocity of impeller, $D_A$ the impeller diameter, $\mu$ the fluid dynamic viscosity, $v$ is the kinematic viscosity of the liquid, $N_p$ the power number of stirrer (Holland and Chapman 1966), and $V$ the volume of the stirring bath.
2. In the pipe

   The Reynolds number for pipe flow is

$$R_e = \frac{\rho \times v_0 \times D_0}{\mu} \tag{4}$$

   According to Eirich (1967) and Matsuo and Unno (1981), the average shear rate for laminar pipe flow is

$$G = \frac{2Q}{\pi \times R_0^3} = \frac{2v_0}{R_0} \tag{5}$$

   According to Camp and Stein (1943), the average shear rate for transitional and turbulent pipe flow is

$$G = \sqrt{\frac{f \times v_0^3}{v \times 8R_0}} \tag{6}$$

where $\rho$ is the fluid density, $v_0$ the mean flow velocity in pipe, $D_0$ the internal diameter of pipe, $\mu$ the fluid dynamic viscosity, $Q$ is the flow rate in pipe, $R_0$ the internal radius of pipe, $v$ the kinematic viscosity of liquid, and $f$ the friction factor (Moody 1944) as

$$f = 0.316 \times R_e^{-0.25} \tag{7}$$

Flocculation of clay particles and EPS molecules in suspension took place in the PSA's liquid bath where continuous stirring caused collisions of clay to clay and clay to EPS molecules. At the same time, the suspension in the liquid bath was circulated in the pipe circulation system. For all particle size analyses, sufficient time (usually 15–20 min) was allowed for the clay suspension in the circulation system to reach a steady state (i.e., no further significant change in the measured PSD curves even for a prolonged period of liquid circulation). As illustrated in Fig. 4, no significant change was observed in the PSD curves captured at a circulating time of 6, 12, and 18 min for a typical clay–EPS sample, which validated that the flocculation process was stabilized even for prolonged circulation. After validating that a steady state was reached, particle size analysis was then conducted in the Cilas PSA. The following sets of experiments were performed, each with its specific purposes:

1. To obtain the intrinsic PSD, the two clays were dispersed in DI water, EA, NaHMP solution (in DI water), and in dry mode. To achieve better dispersion, the built-in ultrasound disperser was turned on for this process, and the stirrer and pump were running at a speed of 180 and 30 rpm, respectively.
2. To investigate the effect of some microbial EPS on the flocculation of the two expansive clays, each of the three EPS was first dissolved in 50 mL DI water assisted by a magnetic stirrer for 30 min mixing (to ensure that the EPS were evenly wetted), followed by mixing the EPS solution into the clay suspensions. For each EPS, three different final EPS concentrations of 1, 10, and 100 μg/g were prepared, leading to totally 9 different EPS solutions and

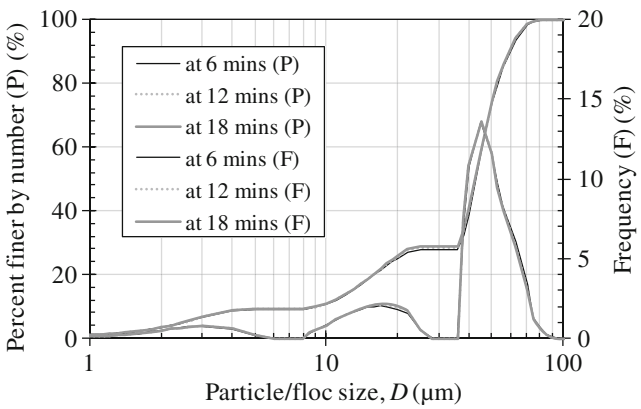


**Fig. 4** Example PSD of a clay sample (Ca-M with 100 μg/g guar gum at high pump speed) after dispersed for 6, 12, and 18 min in the PSA

18 different clay–EPS suspensions. No chemicals were added to these suspensions for further dispersion in this process.

3. To examine the chemical influence (i.e., salinity) on the PSD, the aforementioned sea salt was used to prepare salt water at 0, 5, 10, and 35 ppt salinities to simulate the salinity gradient change from river to ocean in estuaries.
4. To investigate the effect of hydrodynamic conditions on the PSD, the peristaltic circulation pump driving liquid flow in circulation system was run at three different speeds (i.e., low (30 rpm), medium (120 rpm), and high (240 rpm)), while the stirrer's speed remained the same at 180 rpm. Based on a careful calibration, these three pump speeds resulted in the approach flow velocities of 0.15, 0.4, and 0.8 m/s for the liquid inside the circulation system, respectively. To minimize the influence of hydrodynamic shear force on the particle size analysis, the lowest pump speed (i.e., 30 rpm or 0.15 m/s for flow velocity) was selected for evaluating the intrinsic PSD and the influence of biological and chemical factors on the PSD of the two clays.

Finally, in this paper, the particle size obtained by the Cilas PSA is defined as the diameter of equivalent spheres calculated based on the volume moment mean value of multiple particles at a given size range. That is:

$$D = \frac{\sum n \times l^4}{\sum n \times l^3} \tag{8}$$

where $D$ is the mean diameter of all flocs and particles within a given size range, $n$ the number of particles at a fixed size, and $l$ the diameter of a particle or floc.

## 3 Results and discussion

### 3.1 Intrinsic PSD

All PSD curves of the two expansive clays obtained by different dispersion methods are shown in Fig. 5. Both clays exhibit multimodal, lognormal PSD curves consisting of primary particles (submicron to 1–2 μm) and flocculi (10–20 μm) (Lee et al. 2012), except those obtained by the dry dispersion method. Flocculi, a compound word of floc and nuclei (van de Ven and Hunter 1977), consist of strongly bound primary clay particles with a face-to-edge association via Coulomb attraction and have a size of typically 10–20 μm (Lee et al. 2012). Flocculi are the smallest but the densest clay-based flocs which are rarely broken down to the lower level primary particles even at the highest turbulent shear (van de Ven and Hunter 1977), and therefore they may be regarded as a basic and major building unit of flocs (van Leussen 1994). In fact, the dry method yields the largest particle sizes of 100 and ~600 μm for the Ca-M and Na-M, respectively. The PSD curve obtained by the dry dispersion method is situated at the rightmost location (Fig. 5), indicating that these two as-received powdery clay samples are not readily dispersed by dry dispersion in air. In other words, their intrinsic PSD cannot be obtained by dry dispersion.

The two as-received clay samples possess some impurities, which are usually greater than clays (Mermut and Cano 2001; Mosser-Ruck and Cathelineau 2004). In fact, according to their Materials Safety and Data Sheets, the Ca-M and Na-M contain 1–5 and 5–10 wt% quartz as impurity, respectively. In addition, some clay particles may be greater than 2 μm. Therefore, the <2 μm fractions of the two samples were also extracted via sedimentation (i.e., gravitational settling for 3.5 hours (Moore and Reynolds 1997)). The leftmost curves in Fig. 5 are obtained from the <2 μm fractions of the two samples, and both curves show the existence of particles of <2–3 μm. This can also serve as an indirect and partial calibration of the Cilas PSA. For Ca-M, the PSD of the <2 μm fraction shows a bimodal distribution with two maxima at 0.6 and 1.8 μm, respectively. The PSD of Na-M's <2 μm fraction exhibits a monomodal distribution with one maximum at 1.6 μm, which agrees well with previous results (e.g., a peak maximum at ~1.3 μm (Theng 1982; Poli et al. 2008)).

The Ca-M has limited swelling in water and remains its layer structure, since Ca-M does not swell beyond a basal spacing of 1.9 nm (Theng 1982) and this spacing is relatively stable under stirring, sonication, or certain pressure (Kjellander et al. 1988; Laird 2006). Thus, each particle is a stack of parallel 2:1 layers (also called "*tactoid*"). However, the basal spacing of Na-M in water can reach as high as 9 nm (Olejnik et al. 1974). Thus, the highly swelling Na-M particles can exfoliate into individual 2:1 layers of ~1.0 nm in thickness. Such thin 2:1 layers (as individual particles) can easily curl up in the circulation system. As a result, the <2 μm fraction of Na-M shows a monomodal distribution.

It is also interesting to compare the PSD of the two clays dispersed in three different solvents: water, alcohol, and NaHMP solution. From Fig. 5a, b, the $D_{50}$ in DI water and alcohol is 12 and 13 μm for Ca-M, and 2.3 and 13 μm for Na-M, respectively. The particle size of both clays in DI water is smaller than that in alcohol, and the difference for Na-M is greater than that of Ca-M. The dielectric constant (at 20–25 °C) of DI water and ethyl alcohol is 80.4 and 24.3, respectively. If the interlayer space of swelling clays were filled with alcohol, the interlayer attraction force (i.e., Coulomb force) would be much stronger, thus preventing the swelling of montmorillonite. In fact, either Na-M or Ca-M does not swell in pure alcohol (Brindley et al. 1969). As mentioned above, Na-M can swell to infinity in water, and hence one single 2:1 layer is a particle. Therefore, Na-M in

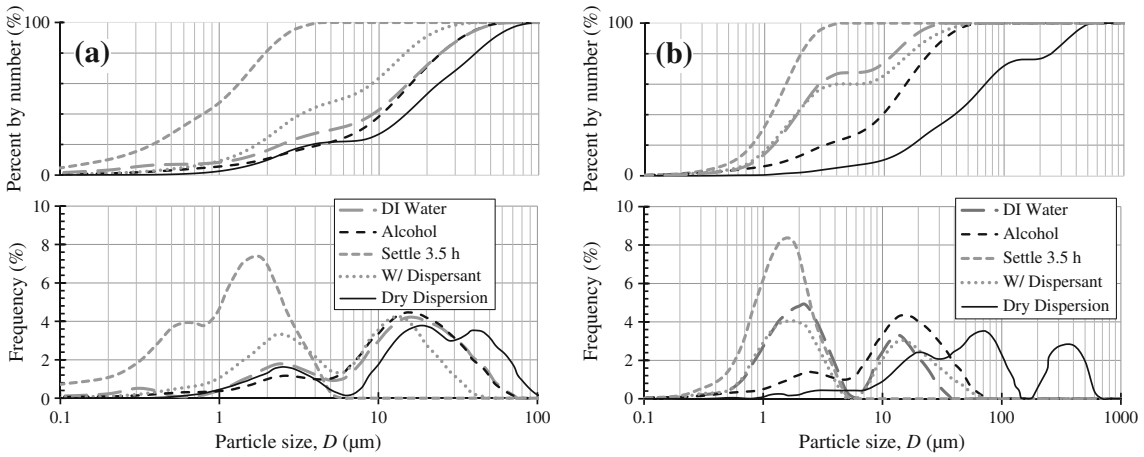


**Fig. 5** Effects of different dispersion methods on the PSD of **a** Ca-montmorillonite and **b** Na-montmorillonite

water exhibits a much finer PSD than in alcohol. For Ca-M, the difference of the PSD in water and alcohol is not significant, even though it swells in water but not in alcohol. This can be reasoned by the fact that the increase in particle size caused by swelling in water is counterbalanced by the decrease in particle size caused by the exfoliation (which in turn is promoted by the flow-induced shearing). In addition, when compared with the <2 μm fraction (i.e., after settling for 3.5 h), each clay in water has almost the same PSD peaks, but with one more larger-sized peak, which is likely due to the existence of impurity, flocs, or bulk sample residue (Pruett and Webb 1993).

Finally, for Ca-M, dispersion in the NaHMP solution results in a much finer PSD than in water, due to partly the cation exchange of $Ca^{2+}$ by $Na^{+}$ and partly the reversal of positive edge charge by $(PO_3^{-})_6$. The former can definitely results in smaller particles, while the latter can reduce the tendency of clay flocculation. For Na-M, the PSD in the NaHMP solution and water are nearly the same. Therefore, adding Na-based dispersant such as NaHMP may generate misleading results for both clay samples, and this is particularly the case for Ca-M.

In summary, due to their swelling nature, both Ca-M and Na-M exhibit different PSD in different dispersion liquids. Dry dispersion in air cannot yield accurate results for clays. The intrinsic particle size of both Ca-M and Na-M should be measured in alcohol or other liquids that should not cause significant swelling. The desired particle size should be determined by dispersion under conditions representative of the environment where the swelling clays are present.

### 3.2 Effects of EPS

The influence of different EPS at various concentrations (all in zero salinity) on the flocculation of expansive clays is summarized in Figs. 6 and 7. All of the three EPS, anionic xanthan, neutral guar, and cationic chitosan, can change the particle size or cause flocculation of both clays. For all three EPS, the Ca-M always exhibits a tri-modal distribution, while the mode of distribution of the Na-M changes with the concentration of xanthan and guar gum. The molecule length of xanthan, guar, and chitosan can be estimated as 1.95–3.47, 4.13–8.25, and 1.24–3.72 μm, respectively, using a published approach (Chang and Cho 2012). Such molecular lengths are in the same size range of clay particles (i.e., mostly <2 μm), and hence flocculation of the two expansive clays through polymer bridging is possible for all of the three EPS.

As shown in Fig. 6a, xanthan gum causes little additional flocculation of Ca-M. As xanthan concentration increases from 0 to 1, 10, and 100 μg/g, the $D_{50}$ of Ca-M increases from 32.4 to 32.8, 32.8, and 33.5 μm (Fig. 7a). Such small changes can be ignored when compared with the influence of the other two EPS. In the primary xanthan structure (Fig. 2a), the anionic side chains are very close to each other, resulting in a high charge density and strong electrostatic repulsion, and hence xanthan keeps a rigid double-helix conformation, which does not facilitate bridging (Labille et al. 2005). Although the optimum concentration of 10 μg/g xanthan used as a flocculating agent for kaolin was reported (Yokoi et al. 1996), the negative layer charge of Ca-M (−0.34, Table 1) is usually much higher than that of kaolin (typically −0.03), and thus the repulsion between Ca-M particle and xanthan molecule is much stronger. Additionally, anionic xanthan molecules cannot enter into the interlayer of swelling clays (Theng 1982; Benchabane and Bekkour 2006). Xanthan gum interacts only with the clay surface principally through an adsorption mechanism, which may be the electrostatic attraction between the negatively charged xanthan and positively charged clay edges at pH <7 (Table 1), and/or the hydrogen bonding between the carboxyl groups on xanthan side chains and the oxygen of the clay lattice (Fig. 8a) (Theng 1970).

For the highly swelling Na-M, the addition of a very small amount of xanthan (1 μg/g) causes no change in the PSD. As xanthan concentration increases to 10 μg/g, the $D_{50}$ increases

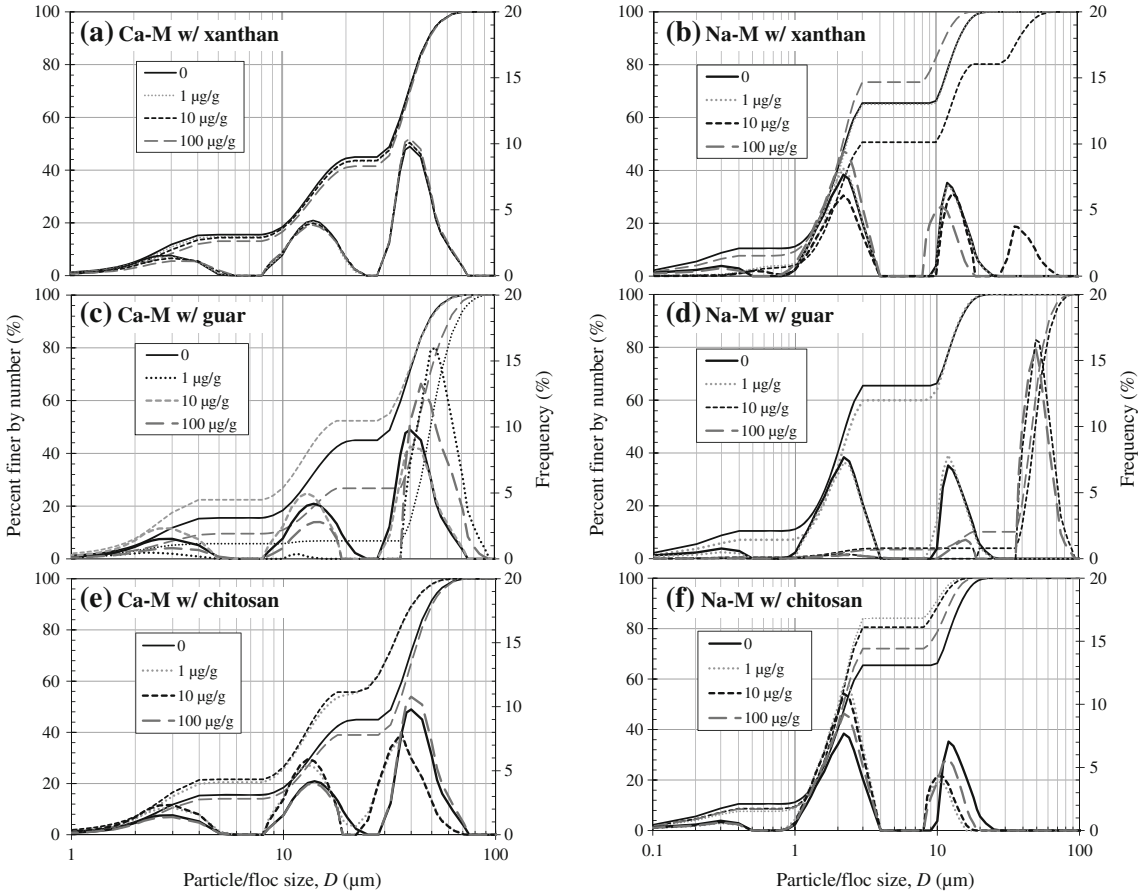


**Fig. 6** Effect of EPS on the PSD of Ca-M and Na-M at different concentrations (low pump speed)

from 2.3 to 2.9 μm and one extra peak appears at ~30–40 μm, while the other two peaks at the smaller size ranges become smaller. This indicates that flocculation takes place, resulting in the formation of coarser flocs that are not previously present. As the xanthan concentration continues to increase to 100 μg/g, the PSD becomes even finer than that of the pure clay with no xanthan, which is further explained below.

The difference in the interaction of Ca-M and Na-M with xanthan is caused by three mechanisms: (1) the negative layer charge of Ca-M is higher than that of Na-M (Table 1), which results in a higher electrostatic repulsion force between Ca-M and xanthan, preventing flocculation of Ca-M with xanthan; (2) the charge location is different: the isomorphous substitution in Ca-M exists only in octahedral sheets, while that in Na-M happens in both octahedral and tetrahedral sheets. The tetrahedral charges form stronger bonds with surface adsorbed cations than the charges in the sandwiched central octahedral sheets (Fig. 1), which promotes the adsorption of xanthan to Ca-M through cation bridging via divalent $Ca^{2+}$, particularly in the presence of a background electrolyte (Dontsova and

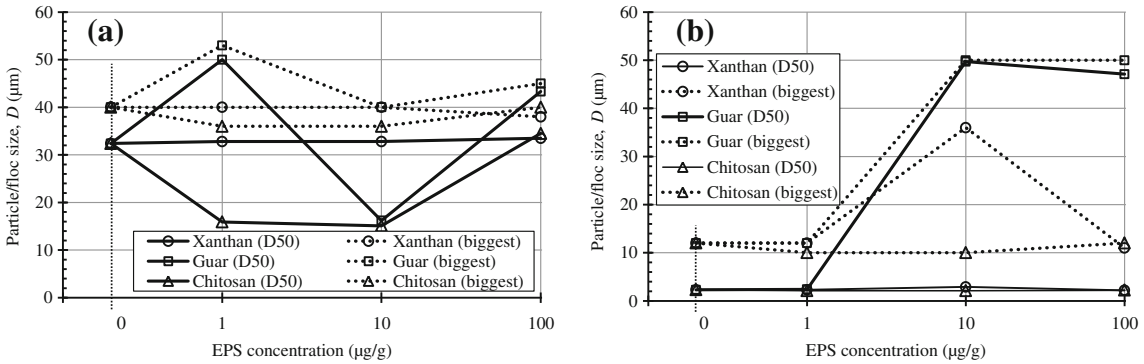


**Fig. 7** The mean particle size ($D_{50}$) and largest floc size of **a** Ca-M and **b** Na-M with the EPS at different concentrations

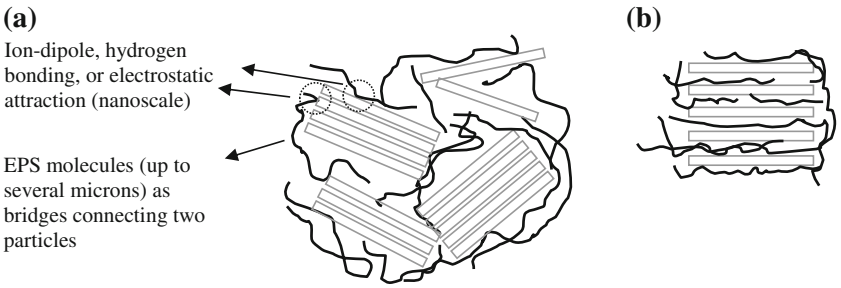


**Fig. 8** Schematic diagram showing clay and EPS interaction: **a** EPS-facilitated flocculation; **b** intercalation of EPS into the swelling clay

Bigham 2005). For the highly swelling Na-M, since each 2:1 layer is an individual particle, more cations expose to water and hence attract the anionic parts of xanthan, which facilitates the flocculation at lower xanthan concentrations; (3) the unbalanced charge of the two clays are totally different, −0.04 for Ca-M and +0.025 for Na-M (Table 1). The negative unbalanced charge of Ca-M bestows the dominance of repulsion between xanthan. The small amount of positive unbalanced charge (i.e., caused by adsorbed cations) tends to attract and be balanced by the negative xanthan at low concentrations, which promotes the flocculation. However, in the high EPS concentrations (e.g., 100 μg/g), the negative charge density increases and the repulsion between particles also increases, preventing particles from flocculation as discussed in the previous two mechanisms. Such a reduction in the degree of flocculation may also be caused by the higher viscosity of the xanthan solution with a higher concentration, which can exert a higher flow-induced shear force on flocs, leading to more floc breakup.

The neutral guar gum significantly changes the PSD of both clays by generating the largest flocs (e.g., up to 100 μm, Fig. 6c, d). For Ca-M, as the guar concentration increases, the PSD curve moves left, then right, and then left again. The highest degree of flocculation with a $D_{50}$ of 50 μm occurs at a concentration of 1 μg/g, while the lowest one with a $D_{50}$ of 16.2 μm at a concentration of 10 μg/g (Fig. 7a). The $D_{50}$ of Ca-M at a guar concentration of 100 μg/g is 43.3 μm. For Na-M, the two intermediate concentrations (i.e., 10 and 100 μg/g) facilitate a higher degree of flocculation with $D_{50}$ increasing from 2.3 to 49.7 and 47.1 μm, respectively. At a lower guar concentration of 1 μg/g, the Na-M slightly increases the particle size with $D_{50}$ increasing from 2.3 to 2.4 μm. The higher degree of flocculation in Ca-M may be caused by the intercalation of guar molecules into the swelling clays (Fig. 8b) (Theng 1982) together with the long-range polymer bridging and short-range ion-dipole interaction or hydrogen bonding between the hydroxyl groups of guar and the oxygen on clay surface (Fig. 8a) (Nugent et al. 2009), while the flocculation of Na-M and guar only results from the latter one. In addition, the molecule length of guar is the longest among the three EPS, which is the main reason for the generation of largest clay–EPS flocs.

Chitosan is insoluble in a neutral or alkaline aqueous solvent, but its amino functional groups are partly charged, resulting in the change of the two clays' PSD. Although the flocculation of clays caused by chitosan at a natural pH is not significant (Chen and Chung 2011) (Figs. 6e, f), for both clays with the addition of chitosan, the particle size initially decreases at a concentration of 1 μg/g, and then increases at a concentration of 10 to 100 μg/g, The $D_{50}$ of Ca-M decreases from 32.4 to 15.0 μm for 1 and 10 μg/g chitosan concentrations, but increases to 34.5 μm at 100 μg/g. The $D_{50}$ of Na-M changes from 2.3 to 2.1 and 2.2 μm as the chitosan concentration increases. The largest-size peak of the two clays also shows the same trend of change. At a very low concentration, the positively charged chitosan molecules are adsorbed only onto the outer surface of particles or flocs, which results in partial separation of flocs (He and Horikawa 2000) and hence a decrease in floc size. The positive charge of chitosan can neutralize the negative charge on clay surface (Ghimici and Nichifor 2009), and its molecules can also enter the interlayer space of swelling clays (Theng 1982). Therefore, as the chitosan concentration increases, the clay surface becomes saturated with adsorbed chitosan, and the excessive chitosan molecules re-flocculate the separated small particles or flocs through polycationic bridging as the long-range interactions as well as electrostatic attraction as the short-range interactions (Fig. 8a), resulting in an increase in floc size.

### 3.3 Effects of salinity

As the salinity increases, the basal spacing of swelling montmorillonite may decrease by several angstroms (Posner and Quirk 1964), which results in a slight decrease in particle size. On the other hand, according to Derjaguin–Landau–Verwey–Overbeek (DLVO) theory (Derjaguin and Landau 1941; Verwey and Overbeek 1948), the interaction between charged clay particles is a summation of van der Waals attraction and electrostatic repulsion due to double layer (DL) of counterions on clay surface, which can be compressed by increasing the cationic concentration of the environment. Thus, the addition of salt can decrease the electrostatic repulsion between montmorillonite particles and cause further flocculation or size increasing. These two competitive mechanisms co-exist in a

saline clay suspension, resulting in particle size variations with salinity. For different types of montmorillonite and different salinities, the one that dominates flocculation may be different.

The characteristic length of the DL thickness, Debye length ($t_D$), on clay surface can be estimated by using the following equation (Block 1978):

$$t_D = \sqrt{\frac{\varepsilon_0 \times \varepsilon \times k \times T}{\sum_{j=1}^{N} n_j \times q_j^2}} \quad (9)$$

where $\varepsilon_0$ is the permittivity of vacuum, $\varepsilon$ the dielectric constant, $k$ Boltzmann constant, $T$ the absolute temperature, and $q_j$ and $n_j$ the valence and mean concentration of the $j$th ion species, respectively.

The dielectric constant of water decreases as the salinity increases, which is 80.4, 79.2, 77.9, and 71.8 for water at 0, 5, 10, and 35 ppt salinities, respectively (Stogryn 1971; Meissner and Wentz 2004). The major ions of the Instant Ocean® sea salt are $Na^+$, $Mg^{2+}$, $K^+$, $Ca^{2+}$, and $Cl^-$, $SO_4^{2-}$, $TCO_2$ (total carbon dioxide) with some other trace ions (Atkinson and Bingman 1998). The DL thicknesses at a salinity of 5, 10, and 35 ppt are estimated as 0.92, 0.64, and 0.32 nm, respectively. Theoretically, the DL in pure water is infinity according to Eq. (2), but the DL thickness of 960 nm in pure water at pH 7 was reported by (Israelachvili 2007).

The effect of salinity on the PSD is shown in Fig. 9. As the salinity increases from 0 to 35 ppt, the particle size of Ca-M decreases with $D_{50}$ decreasing from 32.4 to 24.7 μm, while that of Na-M gradually increases with $D_{50}$ increasing from 2.3 to 28 μm. As discussed previously, in the PSA's liquid circulation system, the limitedly swelling Ca-M maintains its tactoid structure. The presence of salt decreases the basal spacing and hence the thickness of the 2:1 layer particles will be significantly reduced. Additionally, the classical DLVO theory has limitation for predicting clay flocculation (Furukawa and Watkins 2012) that it is not applicable to the limitedly swelling Ca-M (Kjellander et al. 1988). Although the DL thickness deceases from 960 to ~1 nm, the attractive and repulsive forces between Ca-M interlayers may not change. Therefore, the slight decrease in the size of Ca-M in salt water is mainly caused by the decrease of basal spacing, but the change is not so significant. However, for the highly swelling Na-M, the addition of salt eliminates the small clay particles at ~0.3 μm (i.e., the leftmost peak disappears) and results in much larger flocs at ~35 μm (i.e., the rightmost peak appears). As the salinity increases, the particle size increases significantly. Thus, the dominant influence of salt on the Na-M's PSD is the repulsive DL thickness decreasing, which facilitates the flocculation of Na-M particles via face-face or face-edge association and other aforementioned mechanisms. As the salinity increases from 0 to 5 ppt, the DL thickness changes dramatically from 960 to 0.92 nm, and hence the $D_{50}$ of the Na-M has the corresponding largest change from 2.3 to 13.0 μm (i.e., by one order of magnitude). As the salinity increases from 5 to 35 ppt, the DL thickness becomes smaller and smaller, and the $D_{50}$ of Na-M keeps increasing from 13 to 28 μm.

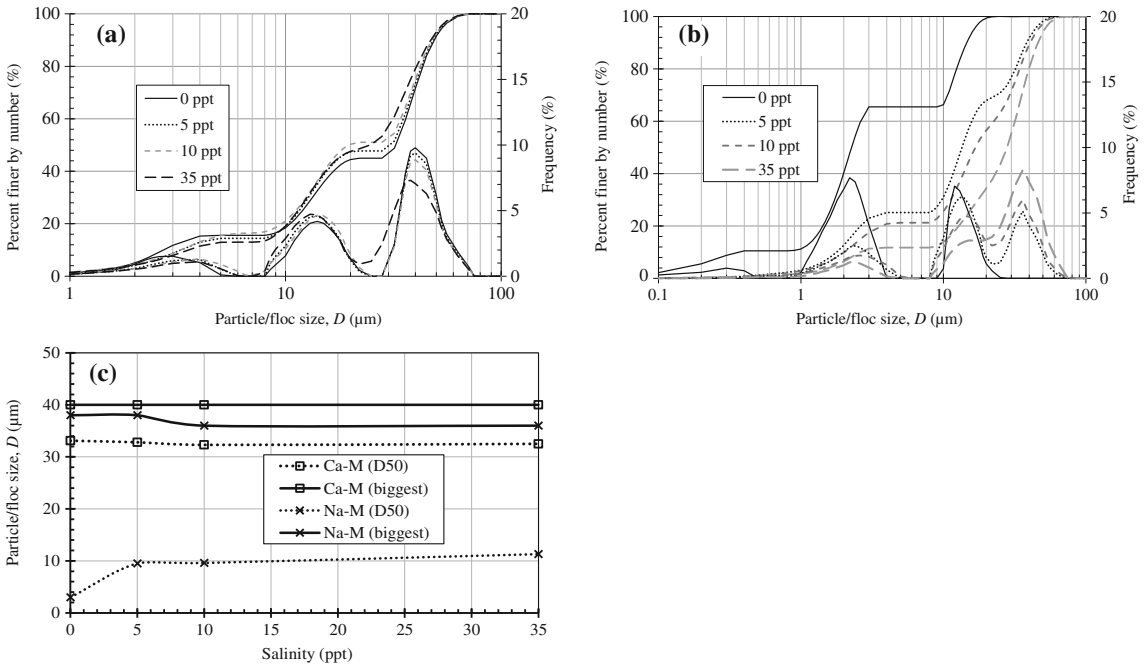


**Fig. 9** PSD of **a** Ca-M and **b** Na-M at 0, 5, 10, 35 ppt salinities (under low pump speed); **c** summary of the mean particle size ($D_{50}$) and largest floc size of both clays at different salinities

### 3.4 Effects of hydrodynamic conditions

The size change and behavior of clay particles and flocs in aqueous flow are due to two competing effects, as shown in Fig. 10: (1) flocculation by the increased collision possibility and hence more adsorption; and (2) breakup into smaller flocs or particles due to the flow-induced shear stress (Yeung et al. 1997; Jarvis et al. 2005; Mietta et al. 2009). At a given hydrodynamic condition which is expected to exert a constant shear force, flocs of similar or higher strength tend to form, because the weaker ones can breakup and re-flocculate until they are strong enough to resist the shear stress exerted by the flow. To evaluate the influence of hydrodynamic factors on the PSD and flocculation behavior of the two expansive clays, the mean size ($D_{50}$) and the largest floc size ($D_m$) are selected from a series of PSD for comparison (Table 2). The hydrodynamic parameters of all clay suspensions in the PSA's liquid circulation system are summarized in Table 3. The concentration of the montmorillonite suspension is 0.4 g/L in this study, which is much smaller than 1.0 g/L, so the general flow behavior is Newtonian (Vali and Bachmann 1988; Guven and Pollastro 1992). The rheological properties of very dilute xanthan, guar, and chitosan solutions (0.0001–0.01 wt% in this study) are different from their relatively higher concentration solutions (e.g., 0.5–10 wt%). Therefore, the dilute EPS solution is also treated as a Newtonian fluid (Fonseca et al. 2011). Their viscosity values (Table 3) were taken from literature, such as xanthan from (He and Horikawa 1996) and chitosan from (He and Horikawa 2000).

The low, medium, and high pump speeds result in different flow velocities and hence different types of flow in the pipe. For the DI water, salt water, and EPS suspension, the pipe flow is laminar ($R_e$ <2,000), transitional (2,000<$R_e$<4,000), and turbulent ($R_e$>4,000) flow for low, medium, and high pump speed, respectively. The corresponding shear rates are also shown in Table 3.

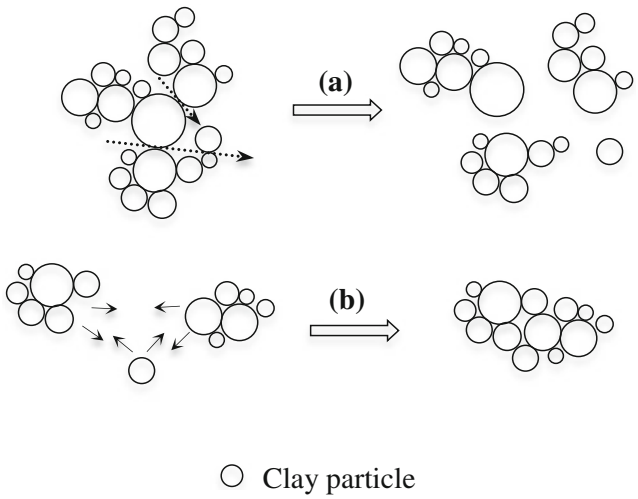


**Fig. 10** Schematic illustration of the effect of shear rate on clay flocculation and floc breakdown in aqueous environments: **a** A floc breaks into smaller flocs or particles due to high shear rate; **b** Flocculation of smaller flocs or particles by the increased collision forces and probability at higher shear rate

In alcohol, under the low and medium speeds, the flow is laminar, and it becomes transitional under the high speed. For both clays, $D_{50}$ and $D_m$ under low and medium pump speeds are almost the same, which may be caused by the fact that clay flocculation is the same in the same type flow. As the pump speed increases, their $D_{50}$ slightly increases, but the largest floc size decreases. The increased fluid shear stress may be high enough to partially break the large-sized well-grown flocs (Tambo and Hozumi 1979), and the separated particles re-flocculate with other micro-flocs, which causes more flocs with larger sizes.

In DI water, the $D_{50}$ of both Ca-M and Na-M increases and then decreases as the flow velocity increases. The value of $D_{50}$ under medium flow velocity is the largest. For swelling clays, the flow turbulence may increase the collision-and-attachment possibility of clays and/or flocs and hence facilitate the flocculation to a certain degree. As the turbulence increases, the floc breakup is dominant, and hence the size of some weaker flocs decreases. The largest floc size of Ca-M remains the same, which means the hydrodynamic shear does not significantly influence the flocculation. The possible reason is that the Ca-M flocs are relatively strong and the flow-induced shear stress is not large enough to break the Ca-M flocs. The $D_m$ of Na-M significantly increases from 12 to 38 μm as the flow velocity increases, which may be due to the presence of turbulent flow that can dramatically help the flocculation and the higher floc strength. These reasons can also explain the floc size change of the two expansive clays in salt water. The only difference is that the size of Na-M flocs in salt water keeps decreasing as the flow velocity increase. The salt-induced flocculation of Na-M may not increase the floc strength accordingly as the floc size increases (Jarvis et al. 2005). Therefore, the appearance of turbulent flow largely decreases the floc mean size when the flow changes from low to medium speeds. As the flow turbulence increases, the floc size decreases. The addition of salt does not help the flocculation of Ca-M, so Ca-M in salt water shows the same behavior as in DI water.

For the EPS-induced flocculation of the two expansive clays, in different type EPS and the different concentrations, the flocs size change caused by the flow velocity is different. Turbulent flow contains various eddies with different size intensities, which affect the flocculation in different ways. In the clay–EPS–water system, eddies may affect both EPS flocculation and floc breakup, and the turbulence may also significantly increase the rate of EPS adsorption on to clay surface (Wågberg and Lindström 1987). Therefore, the size of clay–EPS flocs may also decrease or increase as the flow changes. The hydrodynamic factor does not significantly

**Table 2** Particle or floc size (in micrometer) under different hydrodynamic conditions

| Floc | Pump speed | Intrinsic (in EA) | DI water | Salinity (ppt) | | | EPS concentration (μg/g) | | | | | | | | |
|---|---|---|---|---|---|---|---|---|---|---|---|---|---|---|---|
| | | | | | | | Xanthan | | | Guar | | | Chitosan | | |
| | | | | 5 | 10 | 35 | 1 | 10 | 100 | 1 | 10 | 100 | 1 | 10 | 100 |
| Ca-M $D_{50}$ | Low | 12.7 | 32.4 | 30.3 | 19.7 | 24.7 | 32.8 | 32.8 | 33.5 | 50.0 | 16.2 | 43.3 | 15.9 | 15.1 | 34.5 |
| | Med | 12.9 | 33.1 | 32.8 | 32.3 | 32.5 | 33.5 | 33.0 | 33.2 | 41.1 | 34.0 | 43.2 | 15.0 | 14.8 | 33.4 |
| | High | 13.1 | 32.6 | 32.4 | 31.7 | 32.2 | 32.9 | 32.7 | 33.0 | 35.6 | 34.2 | 42.5 | 15.0 | 14.7 | 33.1 |
| Ca-M $D_m$ | Low | 16 | 40 | 40 | 40 | 38 | 40 | 40 | 38 | 53 | 40 | 45 | 36 | 36 | 40 |
| | Med | 16 | 40 | 40 | 40 | 40 | 40 | 40 | 40 | 45 | 40 | 45 | 36 | 36 | 40 |
| | High | 15 | 40 | 40 | 40 | 40 | 40 | 40 | 40 | 40 | 40 | 45 | 36 | 36 | 40 |
| Na-M $D_{50}$ | Low | 12.3 | 2.3 | 13.5 | 16.8 | 28.0 | 2.3 | 2.9 | 2.2 | 2.4 | 49.7 | 47.1 | 2.1 | 2.1 | 2.2 |
| | Med | 12.3 | 3.0 | 9.5 | 9.6 | 11.3 | 3.0 | 3.0 | 2.2 | 2.4 | 35.2 | 43.9 | 2.1 | 2.1 | 2.3 |
| | High | 12.4 | 2.6 | 2.9 | 3.6 | 10.1 | 2.8 | 2.9 | 2.1 | 2.2 | 14.3 | 39.6 | 2.0 | 2.0 | 2.2 |
| Na-M $D_m$ | Low | 16 | 12 | 36 | 36 | 36 | 12 | 36 | 11 | 12 | 50 | 50 | 10 | 10 | 12 |
| | Med | 16 | 38 | 38 | 36 | 36 | 38 | 38 | 11 | 12 | 40 | 45 | 10 | 10 | 12 |
| | High | 15 | 38 | 38 | 38 | 38 | 38 | 38 | 11 | 12 | 36 | 40 | 11 | 11 | 12 |

change the clay–xanthan and clay–chitosan flocs for both clays, and the small-scale change (<1 μm) can be reasoned using the mechanisms discussed above for the same changes, or these flocs are relatively strong and resistant to breakup. For the clay–guar gum flocs, the size largely decreases (~14 μm) as the flow velocity increases, except for Ca-M in a 10 μg/g guar gum solution. The flocs induced by the flocculation with neutral guar gum are not as strong as with the other two charged EPS. Therefore, the increased shear stress will break the weak flocs and result in a decrease in size. This exception of Ca-M with guar gum is consistent with the above discussion that the strongest Ca-M–guar flocs occur at a concentration of 10 μg/g. The increased turbulence cannot break the flocs. On the contrary, it increases the adsorption of EPS onto clay surfaces, which facilitates flocculation.

Finally, it is worth noting that the shear rates shown in Table 3 exceed those observed in most natural estuaries, with the highest values being greater by 1–2 orders of magnitude (Mietta et al. 2009). As a result, the flocs formed under higher shear rates in the laboratory are expectedly much stronger than those observed in natural estuaries, and their sizes are also usually smaller. Therefore, cautions should be taken in extending the findings of this study to interpret the field observations and the effect of shear rates should not be underestimated. The reason why this study chose such higher shear rates is that the flow rate is limited by the original design

**Table 3** Reynolds number ($R_e$) and average shear rate ($G$) of different solutions or solvents in the stirring bath and flowing pipe (at room temperature)

| Solution or solvent | | Alcohol | Salinity (0–35 ppt) | EPS | | |
|---|---|---|---|---|---|---|
| | | | | Xanthan | Guar[a] | Chitosan |
| Concentration (μg/g) | | NA | NA | 1–100 | 1–100 | 1–100 |
| Dynamic viscosity (mPa s) | | 1.074 | 0.894–1.08 | 1.084–1.092 | 0.894–1.092 | 1.021–1.028 |
| $R_e$ in stirring bath | | 1,377 | 2,097–1,783 | 1,730–1,717 | 2,097–1,717 | 1,836–1,824 |
| $G$ ($s^{-1}$) in stirring bath | | 149 | 184–170 | 167–167 | 184–167 | 172–172 |
| $R_e$ in pipe | Low speed | 726 | 1,091–921 | 899–893 | 1,091–893 | 955–948 |
| | Medium speed | 1,937 | 2,908–2,456 | 2,399–2,380 | 2,908–2,380 | 2,547–2,529 |
| | High speed | 3,873 | 5,817–4,911 | 4,797–4,762 | 5,817–4,762 | 5,093–5,058 |
| $G$ ($s^{-1}$) in pipe | Low speed | 92 | | | | |
| | Medium speed | 293 | 344–324 | 320–319 | 344–319 | 327–326 |
| | High speed | 762 | 893–841 | 831–828 | 893–828 | 849–847 |

[a] The dynamic viscosity of very dilute guar was found between that of DI water and of xanthan solution at the same concentration

of the particle size analyzer used in this study and higher flow rates can yield better dispersion of the clay and biopolymer mixture suspensions.

### 3.5 Implications for sediment analysis

Cohesive sediment particles are transported in the form of flocs in most natural waters (Mietta et al. 2009). Flocculation activity and PSD characteristics of suspended cohesive sediments in different aquatic environments, which change the properties of waterborne constituent particles and affect the transport of particle-bounded contaminants and nutrients, are of essential interest to marine, water, and environmental scientists (Walling and Moorehead 1989; Droppo et al. 1997; Agrawal and Pottsmith 2000; Guo and He 2011). Due to their unique properties, the flocculation and particle size variation of expansive clays are very sensitive to and highly dependent upon the environmental conditions. For sediments rich in expansive clays, in situ sampling and subsequent laboratory characterization should consider the change of the chemistry and biological activities of its aquatic environment (e.g., salinity, EPS production or degradation), as well as the flow conditions. This laboratory-based experimental work sheds instructive lights on the flocculation and PSD variation of expansive clays in fresh water with and without EPS as well as in salt water of varying salinities. The results are expected to help understand the natural floc composition along with the dynamics and mechanisms of flocculation for field monitoring and numerical modeling of cohesive sediment flocculation and transport, particularly under varying aquatic chemical and hydrodynamic conditions.

Compared with non-swelling clays such as kaolinite and illite, the expansive ones are more sensitive to the environmental chemistry and hydrodynamic conditions, such as the polarity of solvent molecules and the presence of salt with different ions. For non-expansive clays, their PSD are also expected to vary with chemical, biological, and hydrodynamic factors that can promote or suppress flocculation. However, a dramatic difference is that these clays usually have a constant intrinsic PSD, or their primary particles have fixed sizes, while the expansive clays may exhibit different intrinsic or primary particle sizes due to swelling (i.e., particle thickness increases), partial or complete exfoliation (i.e., reduction in particle thickness), or interlayer intercalation of relatively large molecules (e.g., certain EPS). Moreover, the surface charges of expansive clays differ from their non-swelling counterparts, resulting in different surface reactivity and other chemical properties. This may lead to the formation of flocs with strength different from that of non-expansive clay flocs. Therefore, further work is warranted to characterize the strength of flocs formed by both expansive and non-expansive clays in different aquatic environments.

## 4 Conclusions

The PSD of two expansive clays, a Ca- and a Na-montmorillonite, under different dispersion methods and different chemical reagents were evaluated. The intrinsic PSD of these two expansive clays were obtained using highly purified ethyl alcohol, which is a less polar solvent inhibiting clay swelling. The two clays both show a bimodal lognormal distribution with particle sizes ranging from 0.2 to 50 μm with a $D_{50}$ of ~13 μm.

The influence of different types of EPS at varying concentrations, different salinities, and hydrodynamic factors on the two clays' flocculation and hence PSD were also characterized. Anionic xanthan gum, neutral guar gum, and cationic chitosan can induce different degrees of flocculation for the two clays through long-range polymer bridging. Xanthan and guar can significantly increase the particle size of Na-M (e.g., from ~10 to ~50 μm for the largest flocs) and generate a higher degree of flocculation, while chitosan decreases the particle size of both clays, owing to the formation of more compacted flocs resulted from polycationic polymer bridging. Increase in salinity facilitates the flocculation of Na-M by decreasing the repulsive electrical double layer thickness, while the particle size of limitedly swelling Ca-M is slightly reduced, which may be resulted from the basal spacing suppression. The flocculation of the two clays under laminar, transitional, and turbulent flows was also evaluated. Generally, the turbulence associated with higher shear rates facilitates the flocculation to different degrees of Ca-M in all of the studied conditions, while the Na-M floc size decreases to certain degrees when the shear rate increases. Therefore, the limitedly swelling Ca-M tends to form relatively stronger and larger flocs than the highly swelling Na-M.

**Acknowledgements** This work was partially supported by the Office of Naval Research (award no. N00173-10-1-G013) under program element number 0601153N. GZ was partially supported by the Overseas Collaboration Award of NSFC (grant no. 51128901). XT received the LSU Graduate School Economic Development Assistantship and a Supplement Award. The facilities used in this study were purchased using the fund from the Louisiana Board of Regents Enhancement Program.

## Notations

| | |
|---|---|
| $D_0$ | Internal diameter of pipe |
| $D$ | Mean diameter of all flocs and particles within a given size range |
| $D_A$ | Impeller diameter |
| $\varepsilon_0$ | Permittivity of vacuum |
| $\varepsilon$ | Dielectric constant |
| $\overline{\varepsilon}$ | Average turbulent energy dissipation per unit time and mass |
| $f$ | Friction factor |

| | |
|---|---|
| $G$ | Average shear rate |
| $k$ | Boltzmann constant |
| $l$ | Diameter of a particle or floc |
| $n$ | Number of particles at a fixed size |
| $n_j$ | Mean concentration of the $j$th ion species |
| $N_p$ | Power number of stirrer |
| $\Omega$ | Angular velocity of impeller in the stirring bath of PSA |
| $\rho$ | Fluid density |
| $q_j$ | Valence of the $j$th ion species |
| $Q$ | Flow rate in pipe |
| $R_0$ | Internal radius of pipe |
| $R_e$ | Reynolds number |
| $t_D$ | Debye length |
| $T$ | Absolute temperature |
| $\mu$ | Fluid dynamic viscosity |
| $v_0$ | Mean flow velocity in pipe |
| $v$ | Kinematic viscosity of the liquid |
| $V$ | Volume of the stirring bath of PSA |

## References


Agrawal YC, Pottsmith HC (2000) Instruments for particle size and settling velocity observations in sediment transport. Mar Geol 168: 89–114

Atkinson MJ, Bingman C (1998) Elemental composition of commercial seasalts. J Aquaric Aquat Sci 8:39–43

Benchabane A, Bekkour K (2006) Effects of anionic additives on the rheological behavior of aqueous calcium montmorillonite suspensions. Rheol Acta 45:425–434

Block LP (1978) A double layer review. Astrophysics and Space Science 55:59–83

Brindley GW, Wiewiora K, Wiewiora A (1969) Intercrystalline swelling of montmorillonite in some water-organic mixtures. Am Mineral 54: 1635–1644

Camp TR, Stein PC (1943) Velocity gradients and internal work in fluid motion. Journal of the Boston Society of Civil Engineers 30:219–237

Chang I, Cho G (2012) Strengthening of korean residual soil with β-1,3/1,6-glucan biopolymer. Constr Build Mater 30:30–35

Chang TS, Joerdel O, Flemming BW, Bartholoma A (2006) The role of particle aggregation/disaggregation in muddy sediment dynamics and seasonal sediment turnover in a back-barrier tidal basin, east frisian wadden sea, southern north sea. Mar Geol 235:49–61

Chen CY, Chung YC (2011) Comparison of acid-soluble and water-soluble chitosan as coagulants in removing bentonite suspensions. Water Air Soil Pollut 217:603–610

D422-63, A.S. (2007) Standard test method for particle-size analysis of soils. Pp., D422-63,ASTM International, West Conshohocken, PA, United States.

Derjaguin B, Landau L (1941) Theory of the stability of strongly charged lyophobic sols and of the adhesion of strongly charged particles in solutions of electrolytes. Acta Physico chemica URSS 14:633

Devine SB, Ferrell RE, Billings GK (1972) A quantitative x-ray diffraction technique applied to fine-grained sediments of the deep gulf Mexico. J Sediment Petrol 42:468–475

Dontsova KM, Bigham JM (2005) Anionic polysaccharide sorption by clay minerals. Soil Sci Soc Am J 69:1026–1035

Droppo IG, Leppard GG, Flannigan DT, Liss SN (1997) The freshwater floc: a functional relationship of water and organic and inorganic floc constituents affecting suspended sediment properties. Water Air Soil Pollut 99:43–53

Eirich FR (1967) Rheology: theory and applications. Academic Press, New York

Fonseca P, Dekker RFH, Barbosa AM, Silveira JLM, Vasconcelos AFD, Monteiro NK, Aranda-Selverio G, da Silva MDC (2011) Thermal and rheological properties of a family of notryosphaerans produced by botryosphaeria rhodina mamb-05. Molecules 16:7488–7501

Furukawa Y, Watkins JL (2012) Effect of organic matter on the flocculation of colloidal montmorillonite: a modeling approach. Journal of Coastal Research 28(3):726–737

Gerbersdorf S, Westrich B, Paterson D (2009) Microbial extracellular polymeric substances (eps) in fresh water sediments. Microb Ecol 58:334–349

Ghimici L, Nichifor M (2009) Flocculation properties of some cationic polysaccharides. Journal of Macromolecular Science Part B-Physics 48:106–113

Guo L, He Q (2011) Freshwater flocculation of suspended sediments in the Yangtze River, China. Ocean Dyn 61:371–386

Gupta BS, Ako JE (2005) Application of guar gum as a flocculant aid in food processing and potable water treatment. Eur Food Res Technol 221:746–751

Guven N, Pollastro RM (1992) Clay-water interface and its rheological implications. In: Guven N (ed) Molecular aspects of clay-water interactions, 4. The Clay Minerals Society, Aurora

He M, Horikawa Y (1996) Stability of allophane, allophanic clay, and allophane-halloysite floc in aqueous solutions of an anionic exocellular heteropolysaccharide (gum xanthan) from *Xanthomonas campestris*. Soil Science and Plant Nutrition 42: 603–612

He M, Horikawa Y (2000) Partial deflocculation of mutual flocs of allophane and halloysite by xanthan and chitosan and relevance to particle arrangement in the flocs. Soil Science and Plant Nutrition 46:81–87

Hill PS (1998) Controls on floc size in the sea. Oceanography 11:13–18

Hiltabrand RR, Ferrell RE, Billings GK (1973) Experimental diagenesis of Gulf Coast argillaceous sediment. Am Assoc Pet Geol Bull 57: 338–348

Hirst CN, Cyr H, Jordan IA (2003) Distribution of exopolymeric substances in the littoral sediments of an oligotrophic lake. Microb Ecol 46:22–32

Holland FA, Chapman FS (1966) Liquid mixing and processing in stirred tanks. Reinhold Publishing Corporation, New York

Ian WS (1994) Structure-function relationships in microbial exopolysaccharides. Biotechnol Adv 12:393–448

Israelachvili, J.N. (2007) Intermolecular and surface forces, 2nd edn. Elsevier Academic Press, New York

Jarvis P, Jefferson B, Gregory J, Parsons SA (2005) A review of floc strength and breakage. Water Res 39:3121–3137

Kjellander R, Marcelja S, Pashley RM, Quirk JP (1988) Double-layer ion correlation forces restrict calcium clay swelling. J Phys Chem 92: 6489–6492

Kleijn WB, Oster JD (1982) A model of clay swelling and tactoid formation. Clay Clay Miner 30:383–390

Labille J, Thomas F, Milas M, Vanhaverbeke C (2005) Flocculation of colloidal clay by bacterial polysaccharides: effect of macromolecule charge and structure. J Colloid Interface Sci 284:149–156

Lagaly G, Ogawa M, Dékány I (2006) Chapter 7.3. Clay mineral organic interactions. In: Faïza Bergaya BKGT, Gerhard L (eds) Developments in clay science, vol. 1, Elsevier, Amsterdam, pp. 309–377

Lagaly G, Ziesmer S (2003) Colloid chemistry of clay minerals: the coagulation of montmorillonite dispersions. Adv Colloid Interf Sci 100:105–128

Laird DA (2006) Influence of layer charge on swelling of smectites. Appl Clay Sci 34:74–87

Lee BJ, Fettweis M, Toorman E, Molz FJ (2012) Multimodality of a particle size distribution of cohesive suspended particulate matters in a coastal zone. Journal of Geophysical Research-Oceans 117(C3)

Luckham PF, Rossi S (1999) The colloidal and rheological properties of bentonite suspensions. Adv Colloid Interf Sci 82:43–92

Matsuo T, Unno H (1981) Forces acting on floc and strength of floc. Journal of the Environmental Engineering Division-Asce 107:527–545

Meissner T, Wentz FJ (2004) The complex dielectric constant of pure and sea water from microwave satellite observations. Ieee Transactions on Geoscience and Remote Sensing 42:1836–1849

Mermut AR, Cano AF (2001) Baseline studies of the clay minerals society source clays: Chemical analyses of major elements. Clay Clay Miner 49:381–386

Mietta F, Chassagne C, Manning AJ, Winterwerp JC (2009) Influence of shear rate, organic matter content, ph and salinity on mud flocculation. Ocean Dyn 59:751–763

Moody LF (1944) Friction factors for pipe flow. Transactions of the ASME 66:671–684

Moore DM, Reynolds, RC (eds) (1997) X-ray diffraction and the identification and analysis of clay minerals, 2nd edn. Oxford University Press, p 378

Mosser-Ruck R, Cathelineau M (2004) Experimental transformation of na, ca-smectite under basic conditions at 150 °C. Appl Clay Sci 26: 259–273

Murray HH (2000) Traditional and new applications for kaolin, smectite, and palygorskite: a general overview. Appl Clay Sci 17:207–221

Majeti NV, Kumar R (2000) A review of chitin and chitosan applications. React Funct Polym 46:1–27

Nair RR, Hashimi NH, Purnachandra, RV (1982) Distribution and dispersal of clay minerals on the western continental shelf of india. Mar Geol 50:M1–M9

Nugent RA, Zhang GP & Gambrell RP (2009) Effect of exopolymers an the liquid limit of clays and its engineering implications. Transportation Research Record 2101:34–43

Olejnik S, Posner AM, Quirk JP (1974) Swelling of montmorillonite in polar organic liquids. Clay Clay Miner 22:361–365

Poli AL, Batista T, Schmitt CC, Gessner F, Neumann MG (2008) Effect of sonication on the particle size of montmorillonite clays. J Colloid Interface Sci 325:386–390

Posner AM, Quirk JP (1964) Changes in basal spacing of montmorillonite in electrolyte solutions. J Colloid Sci 19:798

Pruett RJ, Webb HL (1993) Sampling and analysis of kga-1b well-crystallized kaolin source clay. Clay Clay Miner 41:514–519

Risica D, Dentini M, Crescenzi V (2005) Guar gum methyl ethers—part I. Synthesis and macromolecular characterization. Polymer 46: 12247–12255

Sashiwa H, Aiba SI (2004) Chemically modified chitin and chitosan as biomaterials. Prog Polym Sci 29:887–908

Seo YJ, Seol J, Yeon SH, Koh DY, Cha MJ, Kang SP, Seo YT, Bahk JJ, Lee J, Lee H (2009) Structural, mineralogical, and rheological properties of methane hydrates in smectite clays. J Chem Eng Data 54:1284–1291

Spicer PT, Pratsinis SE (1996) Shear-induced flocculation: the evolution of floc structure and the shape of the size distribution at steady state. Water Res 30:1049–1056

Stogryn A (1971) Equations for calculating the dielectric constant of saline water. Microwave Theory and Techniques, IEEE Transactions on 19:733–736

Tambo N, Hozumi H (1979) Physical aspect of flocculation process—II. Contact flocculation. Water Res 13:441–448

Theng BKG (1970) Interactions of clay minerals with organic polymers—some practical applications. Clay Clay Miner 18:357–362

Theng BKG (1982) Clay-polymer interactions—summary and perspectives. Clay Clay Miner 30:1–10

Theng BKG (2012) Chapter 11—polysaccharides. In: B.K.G. Theng, Ed. Developments in clay science, vol. 4, Elsevier, New York, pp. 351–390

Vali H, Bachmann L (1988) Ultrastructure and flow behavior of colloidal smectite dispersions. J Colloid Interface Sci 126:278–291

van de Ven TGM, Hunter RJ (1977) The energy dissipation in sheared coagulated sols. Rheol Acta 16:534–543

van Leussen W (2011) Macroflocs, fine-grained sediment transports, and their longitudinal variations in the Ems Estuary. Ocean Dyn 61:387–401

van Leussen, W (1994) Estuarine macroflocs and their role in fine-grained sediment transport. Ph.D. Thesis, University of Utrecht, February 1994, Utrecht, The Netherland

van Olphen H (1964) Internal mutual flocculation in clay suspensions. J Colloid Sci 19:313–322

Verwey EJW, Overbeek JTG (1948) Theory of the stability of lyophobic colloids. Elsevier, Amsterdam

Wågberg L, Lindström T (1987) Kinetics of polymer-induced flocculation of cellulosic fibers in turbulent flow. Colloids and Surfaces 27:29–42

Walling DE, Moorehead PW (1989) The particle size characteristics of fluvial suspended sediment: an overview. Hydrobiologia 176–177: 125–149

Winterwerp JC (1998) A simple model for turbulence induced flocculation of cohesive sediment. J Hydraul Res 36:309–326

Wu WJ (2001) Baseline studies of the clay minerals society source clays: colloid and surface phenomena. Clay Clay Miner 49:446–452

Yeung A, Gibbs A, Pelton R (1997) Effect of shear on the strength of polymer-induced flocs. J Colloid Interface Sci 196:113–115

Yokoi H, Shiraki M, Hirose J, Hayashi S, Takasaki Y (1996) Flocculation properties of xanthan produced by *Xanthomonas campestris*. Biotechnol Tech 10:789–792

Yokoi H, Yoshida T, Hirose J, Hayashi S, Takasaki Y (1998) Biopolymer flocculant produced by *Pseudomonas* sp. Biotechnol Tech 12:511–514